Research Article

Transonic Flow Past Morphed Wing

Ambarisha[1], SC Gupta[2]

Abstract

Attempt is made to optimise a wing profile to reduce induced drag in the presence of fixed control surface region, and thereafter transonic flow is progressed over this morphed profile to analyse the presence of shock waves. The displacement of shock wave with increasing Mach number is studied. Encouraging results are obtained. The computer programs are developed in FORTRAN language, and Gfortran complier of Fedora-12 Operating System is used to run these programs. Fedora-12 is supported on LINUX platform of VMware and is an open licence that is available for free-download. The programs are run on a 64 bit double precision Laptop.

Keywords: 3-D Aerofoil, Control surface, Lift coefficient, Pressure difference coefficient, Induced drag, Lagrange multipliers, Morphing, Transonic Flow

Nomenclature

A = Panel Area

a, af = Influence coefficients

b = Semi span

c = Local chord length

c_f = Local flap chord length

Cd_i = Induced drag coefficient

C_L = Lift coefficient

ΔCp = Pressure difference coefficient

D = Induced drag

L = Lift

M = Mach number of free stream

m = Number of panels on trailing edge flap

n = Number of chordwise and also the number of span wise panels

N = Total number of panels on wing (n^2) including the trailing edge flap

[1]PG Student, [2]Professor and Head, Department of Aeronautical Engineering, MVJ College of Engineering, Bangalore, Karnataka, India.

Correspondence: SC Gupta**,** Department of Aeronautical Engineering, MVJ College of Engineering, Bangalore, Karnataka, India.

E-mail Id: satish_chander_gupta@yahoo.co.in

Orcid Id: http://orcid.org/0000-0003-2648-6611

How to cite this article: Ambarisha, Gupta SC. Transonic Flow Past Morphed Wing. *J Adv Res Aero SpaceSci* 2017; 4(3): 1-12.

ISSN: 2454-8669

U = Free stream velocity

u, v, w = Three components of perturbed velocities in the x, y, and z directions

x, y, z = Cartesian co-ordinates in geometric plane, x is chordwise, y is spanwise and z is vertical

dz/dx = Aero foil camber (Zx)

φ = velocity potential

a = Angle of attack

b = $\sqrt{|1 - M^2|}$

Ù = Panel leading edge sweep

γ = circulation

ρ = density

Suffix

i = Control point, also grid point index in x-axis

j = Panel index, also grid point in h-axis

k = Grid point in z-axis

fix = Fixed slopes

le = Leading edge

te = Trailing edge

Introduction

Aerodynamic optimum shape can be considerably different at different flight conditions, thereby requiring camber change for optimum aerodynamic efficiency. Trailing edge devices when deflected produce camber change that is associated with drag penalty. Moreover their camber change is not smooth. Camber-morphing aerofoils aim to achieve their camber change in a smooth way, to potentially reduce the drag penalty.[1-4] Optimum shape generation using Radial Basis Functions has been attempted in the past. There is large number of Radial Basis Functions to choose from.

Single multi-objective optimisation is progressed here-in for drag minimisation solution and the effect of transonic flow is studied on such profiles. In this paper 3-d aerofoil shapes for high speed application are developed. The induced drag is minimised and optimal camber obtained. High subsonic Mach number is taken. Objective function for drag minimum is formed through Lagrange multipliers. Circulation is determined to support minimum drag, from where total lift and drag values are computed. The aerofoil thickness is superimposed on this optimal camber lines. Thereafter transonic flow computations are progressed. Transonic flow computations are based upon transonic small perturbation equation. Morph details are determined for one typical flight condition. By varying the input data regarding flight parameter different camber shapes can be generated. Encouraging results are obtained with this application.

The programs are developed in FORTRAN language and executed through Gfortran complier which is available on Fedora Operating System (OS). This OS is supported on LINUX platform through VMware and is available as open license free download.

Following commands complies and creates a binary ready for executions.

```
gfortran -o program name   program name.f
```

Following command executes the program file:

```
./program name<input file name
```

Following commands are available in the Gfortran compiler.

pwd - Present working directory

cd - Change directory

mk dir - Create directory

vi program.f - Opens the program in vi editor

:q - Quit editor mode

se nu - Gives no sequence for entire file

rm - Program name removes a program

Gfortran - o-program name program name.f - Compiles and creates a binary ready for execution

/program name- Executes the program file

The wing configuration so generated is modelled through CATIA, and ANSYS-FLUENT utilised for flow analysis. Excellent agreement of this work with results from FLUENT is seen.

Mathematical Modelling

Morphing

It refers to optimization in a confined region for a given flight condition or control surface deflection. In our work control surface is taken as part of given aerofoil and it is kept at zero angle of deflection. Wing is represented

by a large number of constant pressure panels to model circulation i.e., the lift effects. These panels are taken for estimation of pressure difference coefficient. Impermeable surface boundary condition option is used. Linearized flow conditions within the frame work of potential flow theory are handled. Chordwise paneling is done (Fig. 1). The program uses vortex panel method to calculate downwash by satisfying tangential flow boundary condition. Control points for determining downwash are taken at 95% of local panel chords. Half of the wing is considered, another half of wing is imaged by the following expression:

$$y(image) = -y_k - y_p \quad (1)$$

The subscript p refers to panel and subscript k refers to control location. Panel circulation (γ) is determined through tangential flow boundary condition and pressure difference co-efficient is given by $\Delta Cp = 2\gamma / U$. Lift is determined through integration of ΔCp over the chord and span. The program thus developed in FORTRAN generates the output matrix consisting of pressure difference coefficients from where lift and drag are determined. Having determined lift over the known mean line of aerofoil, the matrix of constrained optimization is developed to restrain variation in lift values and to restraint variations in the mean line of control surface. As a result new camber for mean line in the required region is developed. Having determined the pressure difference in this case, the lift, drag and slopes of camber are worked out.

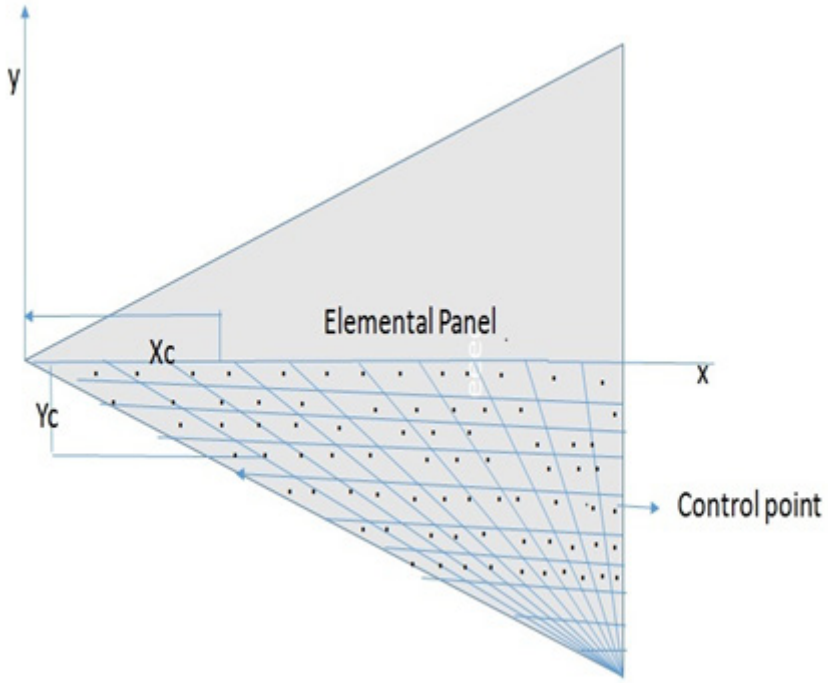

Figure 1.Chordwise paneling and location of control points

Lift is given by Eq. (2):

$$L = \rho U\left[A_1\gamma_1 + \cdots + A_N\gamma_N\right] \quad (2)$$

Lift effects are simulated by a spread of vortex sheet (circulation strength) i.e., Eq. (3).

$$\gamma = u_1 - u_2 \quad (3)$$

Where u_1 and u_2 are tangential velocities just above and below the sheet. The value of γ is zero at the trailing edge, this condition namely γ_{te}= 0 is well known as Kutta condition which fixes the accurate value of circulation around an aerofoil with sharp trailing edge. The boundary conditions for impermeable surface are applied to satisfy the tangency of flow, Eq. (4) to refer. The exact boundary condition of normal flow to surface being zero is not available in our case, therefore reduced option of zero normal velocity with restriction of perturbation velocity being very small compared to free stream velocity is applied compressibility correction is applied though parameter β

$$\hat{n}\,\rho\,q = 0, \quad \bar{q} = \left(U + u\right)\bar{i} + v\bar{j} + w\bar{k} \quad (4)$$

$$u < \quad O\left(U\right)$$

$$\hat{n}\,q = 0, \quad \rho\,\bar{q} \approx \left(U + \beta^2 u\right)\bar{i} + v\bar{j} + w\bar{k}$$

ISSN: 2454-8669

$$M^2 u < O(u) \quad (5)$$

Where $\beta = \sqrt{|1 - M^2|}$, and $\hat{n}$ is the normal unit vector to surface, q is the resultant velocity.

The solution of matrix thus developed by satisfying the boundary conditions results in lift value that is required as a constraint for our objective function.

Objective function (F) for the drag minima is formed as below, where $\bar{L}$ is constrained value of lift, i.e. value of lift before optimization, and λ used as Lagrange multiplier[5,6]:

$$F = D + \lambda_0\left(L - \bar{L}\right) + \sum_{l=N-m+1}^{N} \lambda_l \left(\boldsymbol{X}_l - Z\bar{X}_l\right)_{fix} \quad (6)$$

$\boldsymbol{X}^{-}_{fix}$ are the constrained slopes i.e. fixed slopes.

Matrix of optimization given by Eq. (7) is obtained by differentiation of objective function (F) w.r.t circulation.

Expression for drag minima is given by:

$$D_{\min} = \rho U \begin{bmatrix} (a_{1,1}\gamma_1 + \ldots + a_{1,N}\gamma_N)\gamma_1 A_1 + (a_{2,1}\gamma_1 + \ldots. + a_{2,N}\gamma_N)\gamma_2 A_2 \\ + \ldots\ldots\ldots\ldots\ldots + (a_{N,1}\gamma_1 + \ldots. + a_{N,N}\gamma_N)\gamma_N A_N \end{bmatrix}$$

The optimal warp is given by:

$$\boldsymbol{X}_i = (a_{i,1}\gamma_1 + \cdots + a_{i,n}\gamma_n)A_i$$

The solution of this matrix results in the optimum circulation; from where the camber is determined. Thus, most optimum profile for a given region is constructed. The matrix provides the optimum circulation values γ_1 .... γ_N for the minimum induced drag, from where the lift and drag are calculated, and new camber line is determined. Thickness of aerofoil is superimposed on these developed camber lines.

$$\begin{bmatrix} 2A_1a_{1,1} & \cdots & A_1a_{1,N}+A_Na_{N,1} & A_1 & \boldsymbol{i}_{N-m+1,1} & \cdots & \boldsymbol{i}_{N,1} \\ \vdots & \cdots & \vdots & \vdots & \vdots & \cdots & \\ \vdots & \cdots & \vdots & \vdots & \vdots & \cdots & \\ \vdots & \cdots & \vdots & \vdots & \vdots & \cdots & \\ A_Na_{N,1}+A_1a_{1,N} & \cdots & 2A_Na_{N,N} & A_N & \boldsymbol{i}_{N-m+1,N} & \cdots & \boldsymbol{i}_{N,N} \\ A_1 & & A_N & 0 & & & \vdots \\ \boldsymbol{i}_{N-m+1,1} & \cdots & \boldsymbol{i}_{N-m+1,N} & \vdots & & & \vdots \\ \vdots & & \vdots & \vdots & & & \vdots \\ \vdots & & \vdots & \vdots & & & \vdots \\ \boldsymbol{i}_{N,1} & \cdots & \boldsymbol{i}_{N,N} & 0 & 0 & 0\ 0 & 0 \end{bmatrix} \times \begin{bmatrix} \gamma_1 \\ \gamma_2 \\ \vdots \\ \vdots \\ \gamma_N \\ \lambda_{N-m+1} \\ \lambda_{N-m+2} \\ \vdots \\ \vdots \\ \lambda_N \end{bmatrix} = \begin{bmatrix} 0 \\ \vdots \\ \vdots \\ \vdots \\ \overline{L} \\ \left(\bar{\boldsymbol{X}}_{N-m+1}\right)_{fix} \\ \vdots \\ \vdots \\ \left(\overline{\boldsymbol{X}}_N\right)_{fix} \end{bmatrix}$$

Transonic Flow

Optimization can push transonic drag rise closer to Mach 1 and flight duration gets shortened by increasing free stream Mach number. Therefore, computations of transonic flow is progressed on the developed aerofoils to check for presence of shock waves in a bid to establish critical Mach number where the drag rise is high.[7] Transonic small perturbation equation below is used, where γ is the ratio of specific heats:

$$\left[\left(1 - M^2\right)\phi_x\right]_x + \phi_{yy} + \phi_{zz} = 0 \quad (8)$$

Where $1 - M^2 = 1 - M_\infty^2 - K\phi_x$ and $K = \frac{2}{U}\left[1 + \frac{\gamma - 1}{2} M_\infty^2\right] M_\infty^2$

Equation is solved with finite difference methodology with line relaxation process. Mass conservative form is useful for accuracy of results, i.e., Eqn. (9) to refer.

Much of the nonlinearity comes from the second derivative terms.

$$p_{i,\ j,\ k} + q_{i,\ j,\ k} + r_{i,\ j,\ k} - = 0\left(\mu_{i,\ j,\ k}\ p_{i,\ j,\ k} - \mu_{i-1,\ j}\ p_{i-1,\ i,\ k}\right) \quad (9)$$

m provide the conservation in mass flax.

Where p, q and r are the central difference operators

$\mu_{i-1,\ j,\ k} = 0, \mu_{i,\ j,\ k} = 0$ for elliptic region

$\mu_{i-1,\ j,\ k} = 1, \mu_{i,\ j,\ k} = 1$ for hyperbolic region

$\mu_{i-1,\ j,\ k} = 0, \mu_{i,\ j,\ k} = 1$ for sonic point operator

$\mu_{i-1,\ j,\ k} = 1, \mu_{i,\ j,\ k} = 0$ for shock point operator

The computational plane from the geometric plane is developed in the following manner.

$$\xi = \frac{x - x_{1e}}{x_{te} - x_{le}} \quad \eta = y, \zeta = z \tag{10}$$

Using this transformation, the values of ϕ derivatives can be written as below:

$$\phi_x = \phi_\xi \, \xi_x$$

$$\phi_y = \phi_\xi \, \xi_y + \phi_\eta$$

$$\phi_z = \phi_\zeta$$

$$\phi_{x\,x} = \left(\phi_\xi \quad \xi_x\right)_\xi \quad \xi_x$$

$$\phi_{y\,y} = \left(\phi_\xi \quad \xi_y + \phi_\eta\right)_\xi \, \xi_y + \left(\phi_\xi \quad \xi_y + \phi_\eta\right)_\eta$$

$$\phi_{z\,z} = \phi_{\xi\,\xi}$$

Using these above equations, transonic small perturbation equation (9) is written as equation (12).

$$\left(1 - M^2\right)\left(\phi_\xi \, \xi_x\right)_\xi + \frac{\xi_y}{\xi_x}\left(\phi_\xi \, \xi_y + \phi_\eta\right)_\xi$$

$$+ \frac{1}{\xi_x}\left(\phi_\xi \, \xi_y + \phi_\eta\right)_\eta + \frac{1}{\xi_x}\phi_{\zeta\zeta} = 0 \tag{12}$$

$\xi_x = 1/c$, and $\xi_y = \tan \wedge / c$

$$\left[\left(1 - M^2\right)\xi_x^2 + \xi_y^2\right] \quad \varphi_{\xi\xi} + \xi_y\left(\varphi_{\eta\xi} + \varphi_{\xi\eta}\right) + \varphi_{\eta\eta} + \varphi_{\zeta\zeta} = 0 \tag{13}$$

Condition for elliptic region for equations (12) or (13) is $\left[\left(1 - M^2\right)\xi_x^2 + \xi_y^2\right] > 0$

Condition for hyperbolic region is $\left[\left(1 - M^2\right)\xi_x^2 + \xi_y^2\right] < 0$

The derivatives of ϕ are determined from following equations.

$$\left(\varphi_\eta\right)_\xi = \frac{\varphi_{\eta_{i+1,j,k}} - \varphi_{\eta_{i-1,j,k}}}{\xi_{i+1,j,k} - \xi_{i-1,j\,k}}$$

$$= \frac{\left(\varphi_{i+1,j+1,k} - \varphi_{i+1,j-1,k}\right)}{\left(\xi_{i+1,j,k} - \xi_{i-1,j\,k}\right)\left(\eta_{i+1,j+1,k} - \eta_{i+1,j-1,k}\right)}$$

$$- \frac{\left(\varphi_{i-1,j+1,k} - \varphi_{i-1,j-1,k}\right)}{\left(\xi_{i+1,j,k} - \xi_{i-1,j,k}\right)\left(\eta_{i-1,j+1,k} - \eta_{i-1,j-1,k}\right)} \tag{14}$$

$$\left(\varphi_\xi\right)_\eta = \frac{\varphi_{\xi_{i,j+1,k}} - \varphi_{\xi_{i,j-1,k}}}{\eta_{i,j+1,k} - \eta_{i,j-1,k}}$$

$$= \frac{\left(\varphi_{i+1,j+1,k} - \varphi_{i-1,j+1,k}\right)}{\left(\eta_{i,j+1,k} - \eta_{i,j-1,k}\right)\left(\xi_{i+1,j+1,k} - \xi_{i-1,j+1,k}\right)}$$

$$- \frac{\left(\varphi_{i+1,j-1,k} - \varphi_{i-1,j-1,k}\right)}{\left(\eta_{i,j+1,k} - \eta_{i,j-1,k}\right)\left(\xi_{i+1,j-1,k} - \xi_{i-1,j-1,k}\right)} \tag{15}$$

$$\left(\varphi_\eta\right)_\xi = \frac{\varphi_{\eta_{i,j,k}} - \varphi_{\eta_{i-2,j,k}}}{\xi_{i,j,k} - \xi_{i-2,j,k}}$$

$$= \frac{\left(\varphi_{i,j+1,k} - \varphi_{i,j-1,k}\right)}{\left(\xi_{i,j,k} - \xi_{i-2,j,k}\right)\left(\eta_{i,j+1,k} - \eta_{i,j-1,k}\right)}$$

$$- \frac{\left(\varphi_{i-2,j+1,k} - \varphi_{i-2,j-1,k}\right)}{\left(\xi_{i,j,k} - \xi_{i-2,j,k}\right)\left(\eta_{i-2,j+1,k} - \eta_{i-2,j-1,k}\right)} \tag{16}$$

$$\left(\varphi_\xi\right)_\eta = \frac{\varphi_{\xi_{i,j+1,k}} - \varphi_{\xi_{i,j-1,k}}}{\eta_{i,j+1,k} - \eta_{i,j-1,k}}$$

$$= \frac{\left(\varphi_{i,j+1,k} - \varphi_{i-2,j+1,k}\right)}{\left(\eta_{i,j+1,k} - \eta_{i,j-1,k}\right)\left(\xi_{i,j+1,k} - \xi_{i-2,j+1,k}\right)}$$

$$- \frac{\left(\varphi_{i,j-1,k} - \varphi_{i-2,j-1,k}\right)}{\left(\eta_{i,j+1,k} - \eta_{i,j-1,k}\right)\left(\xi_{i,j-1,k} - \xi_{i-2,j-1,k}\right)} \tag{17}$$

Eq. (13) is transformed into difference equation through above equations and solved by line relaxation process. In the local supersonic region $\left[\left(1 - M^2\right)\xi_x^2 + \xi_y^2\right] < 0$ condition provides the upwind conservation.

Results and Discussions

Following is taken as candidate wing for our studies. Mach number is taken is 0.7, and angle-of-attack is taken as 3^0. Analysis is done for sea level conditions. Flight at a lower pressure altitude is therefore in favour of increased critical Mach number.

Leading edge sweep = 28.0^0 Trailing edge sweep = 14.6^0

Aspect ratio = 7 Taper ratio = 0.35

Aerofoil: NACA 0006

1/3rd of local chords are taken for control surface positioning cf/c = 0.33. Mean line for this symmetrical aerofoil based wing is Zx=0. The 3-d camber in the remaining 2/3rd portion of wing is generated for the above flight conditions. Figure 2 shows the % chordwise camber before and after morphing at y/b/2 span. Camber at aft 1/3rd of local chords remains invariant, as required. Maximum camber is 2% at 30% of

ISSN: 2454-8669

local chord length. Fig. 3 shows camber across the span at three stations. Mid and tip stations, the camber distribution in chordwise direction is same. Peak camber is occurring at 30% at all span stations, and is around 1.8%.

Thickness of NACA 0006 aerofoil are superimposed on this camber line and the resulting pressure distributions obtained and are shown in Figures 4 and 5 for same conditions of Mach number and angle-of-attack.

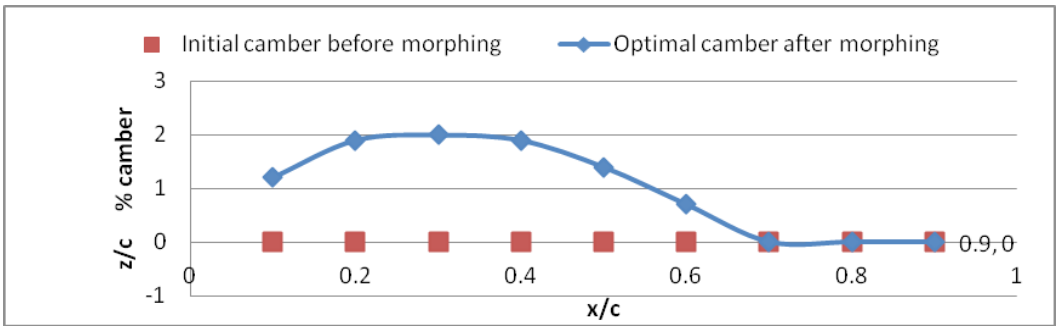

Figure 2.Chordwise % camber distribution at y/b/2 =0.5 station

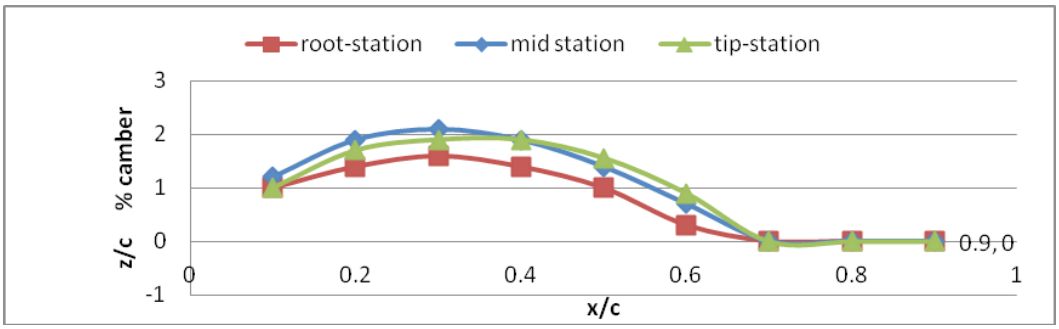

Figure 3.Chordwise % optimal camber distribution across the span, Mach no.= 0.7, a = 3^0

Figure 4 shows the plots before morphing whereas Fig. 5 shows the plots after morphing. Comparing these, large pressure difference is seen as a result of morphing in the interior region of wing. There is shift in adverse pressure gradient towards rear of leading edge of wing and that is in favor of delay in flow separation. There is loss of suction on upper surface and loss of compression on bottom surface aft of 1/3rd of local chord (Fig. 5). Root portion is more affected compared to wing tip areas. This is because of the resistance to flow created by change of camber of control lines. At 40 % of local chords there is peak pressure difference, and this is good from structural design purpose.

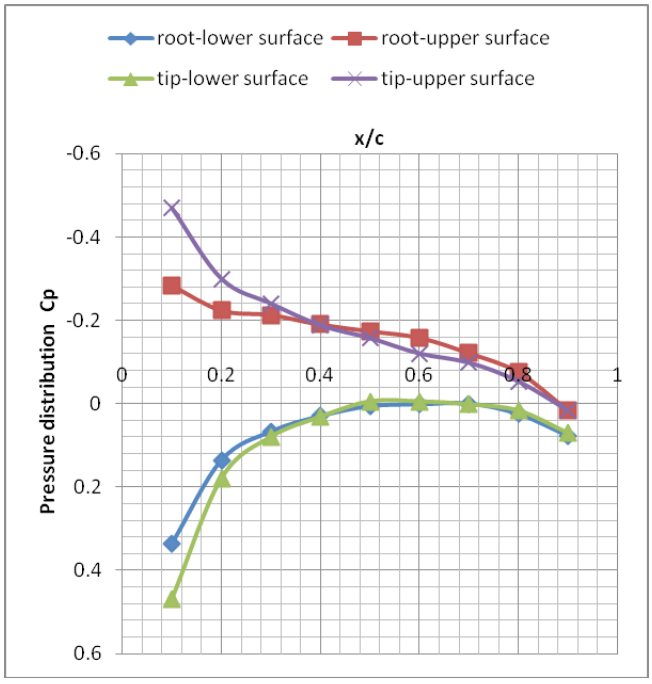

Figure 4.Chordwise pressure plots before morphing

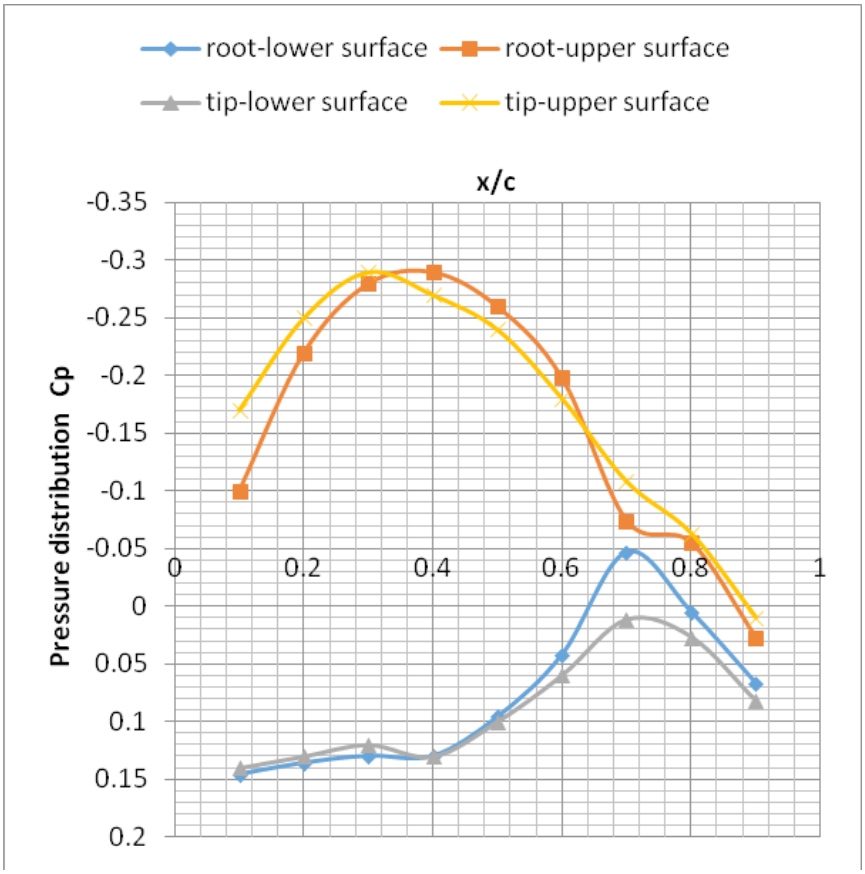

Figure 5.Chordwise pressure plots after morphing

Table 1.% reduction in Induced drag as a result of morphing

C_L	Pre-morph Cd_i	Post-morph Cd_i	Reduction in Cd_i
0.28	0.0146	.007	52.0%

Mach no. = 0.7, a = 3^0

A value of % reduction in induced drag as a result of morphing is shown in Table 1. Substantial drag reduction is seen feasible (note that lift coefficient remains same after the morphing as required).

Now the transonic flow is progressed for free stream Mach numbers of 0.9, and 0.95. Shock is seen present on upper surface. Table 2 and Table 3 show the plots of local Mach numbers on wing upper surfaces for post-morph profiles for Mach number of 0.9 and angles–of–attack of 0^0 and 4^0 respectively. The drop in Mach number below unity from a value above unity is through a shock wave. As the angle-of-attack is increased the shock moves forwards towards trailing edge. This can be seen from comparison of two tables. Towards the wing tips the Mach numbers remain supersonic for angle-of-attack of 4^0; this is because of the larger suction presence at such places. This is reasoned from the fact that there is span wise component of flow due to leading edge sweep that generates greater lift coefficient value at the tips, even though the tip vorticity causes induced angle-of attack to reduce effective angle of attack. Table 4 shows the effect of increase of Mach number to 0.95. Once supersonic the flow is mostly supersonic expect for a small very small pocket that is marked by arrow and is indicative of presence of shock wave. Comparing Tables 2, 3 and 4, it is clear that the effect of increase in Mach number or increase in angle-of-attack is to move the shock wave forwards. Some pressure coefficient details for the combination of Mach number = 0.9 and a = 4^0 are shown in Table 5 for reference. Similarity of shock wave location in Table 3 and Table 5 is evident because of similarity in flow conditions. While the flow condition is same, Table 3 is for post-morph profile while Table 6 is for pre-morph profile. In case of Pre-morph there is virtually no shock as such but from a small value of Mach number greater than one it drops to a value close to lower than one. This appears to be a case of sonic flow prevailing all over the wing.

ISSN: 2454-8669

Table 2.Post-Morph: Free stream Mach number=0.9, a = 0^0

0.908 1.071 1.158 1.136 0.977 0.963 0.954 0.949 0.943
0.898 1.073 1.157 1.057 0.991 0.941 0.926 0.908 0.876
0.888 1.073 1.156 1.045 0.980 0.928 0.917 0.901 0.869
0.880 1.072 1.157 1.030 0.977 0.920 0.912 0.898 0.867
0.871 1.070 1.151 1.039 0.963 0.911 0.907 0.896 0.866
0.863 1.067 1.146 1.042 0.953 0.901 0.903 0.894 0.866
0.856 1.063 1.138 1.027 0.961 0.897 0.899 0.893 0.865
0.848 1.058 1.129 1.021 0.960 0.894 0.898 0.892 0.865
0.839 1.048 1.117 1.015 0.959 0.897 0.898 0.892 0.864
0.829 1.039 1.106 1.012 0.955 0.895 0.897 0.891 0.864
0.829 1.040 1.113 1.032 0.960 0.895 0.898 0.893 0.865
0.828 1.037 1.116 1.054 0.962 0.900 0.901 0.894 0.865
0.828 1.033 1.116 1.084 0.956 0.904 0.904 0.896 0.866
0.831 1.030 1.115 1.083 0.978 0.913 0.908 0.898 0.867
0.834 1.027 1.116 1.070 0.997 0.925 0.915 0.901 0.868
0.838 1.023 1.112 1.086 0.993 0.936 0.921 0.904 0.869
0.845 1.021 1.108 1.085 0.999 0.946 0.926 0.906 0.869
0.860 1.023 1.106 1.080 0.999 0.956 0.928 0.905 0.870
0.881 1.036 1.119 1.106 0.985 0.950 0.918 0.885 0.838

Local Mach numbers on wing upper surface
Rows read chordwise, and column read span wise from tip to tip

Table 3.Post-Morph: Free stream Mach number=0.9, a = 4^0

0.915 1.111 1.215 1.281 1.311 1.077 1.051 1.066 1.057
0.910 1.103 1.227 1.289 1.298 0.943 0.983 1.017 1.029
0.897 1.118 1.225 1.283 1.266 0.897 0.935 0.953 0.941
0.889 1.113 1.232 1.279 1.187 0.908 0.941 0.947 0.920
0.883 1.114 1.229 1.277 1.086 0.946 0.955 0.951 0.917
0.877 1.114 1.227 1.272 1.043 0.942 0.954 0.952 0.917
0.872 1.113 1.222 1.252 1.037 0.931 0.949 0.950 0.916
0.866 1.112 1.214 1.234 1.032 0.927 0.946 0.948 0.916
0.859 1.107 1.200 1.212 1.035 0.927 0.945 0.947 0.915
0.848 1.097 1.188 1.195 1.053 0.914 0.942 0.946 0.915
0.845 1.093 1.192 1.207 1.124 0.884 0.931 0.945 0.916
0.842 1.087 1.190 1.212 1.179 0.887 0.925 0.941 0.916
0.841 1.081 1.186 1.220 1.200 0.916 0.932 0.941 0.916
0.843 1.076 1.182 1.214 1.212 0.956 0.949 0.946 0.916
0.846 1.071 1.181 1.208 1.215 0.994 0.967 0.954 0.918
0.850 1.066 1.175 1.211 1.221 1.024 0.979 0.962 0.919
0.858 1.063 1.170 1.210 1.227 1.059 0.981 0.966 0.921
0.873 1.065 1.167 1.214 1.235 1.093 0.964 0.959 0.922
0.892 1.075 1.177 1.230 1.257 1.156 1.08 1.06 0.981

Local Mach numbers on wing upper surface
Rows read chordwise, and column read span wise from tip to tip

Table 4.Post-Morph: Free stream Mach number = 0.95, a = 4^0

0.893 1.120 1.231 1.306 1.362 1.388 1.383 1.356 1.299
0.891 1.104 1.247 1.325 1.370 1.378 1.248 1.046 1.079
0.878 1.116 1.251 1.326 1.370 1.370 1.036 1.066 1.079
0.871 1.121 1.258 1.325 1.366 1.347 0.975 1.032 1.045
0.865 1.124 1.259 1.328 1.361 1.273 0.955 1.014 0.993
0.861 1.127 1.261 1.328 1.351 1.072 1.058 1.033 0.965
0.858 1.129 1.260 1.315 1.336 1.020 1.034 1.038 0.964
0.854 1.130 1.255 1.304 1.318 1.008 1.015 1.026 0.966
0.848 1.126 1.246 1.287 1.296 1.023 1.003 1.018 0.966
0.841 1.121 1.234 1.268 1.273 1.060 0.981 1.011 0.966
0.838 1.120 1.234 1.273 1.282 1.159 0.941 0.995 0.968
0.835 1.114 1.229 1.273 1.287 1.228 0.964 0.980 0.967
0.832 1.104 1.224 1.277 1.288 1.249 1.071 0.954 0.964
0.833 1.097 1.219 1.268 1.288 1.263 1.220 0.923 0.949
0.836 1.091 1.216 1.261 1.286 1.273 1.257 1.010 0.952
0.841 1.085 1.208 1.261 1.288 1.285 1.272 1.169 0.922
0.849 1.081 1.202 1.257 1.290 1.299 1.291 1.268 1.082
0.862 1.079 1.196 1.256 1.295 1.315 1.313 1.302 1.091
0.879 1.086 1.200 1.266 1.311 1.337 1.340 1.336 1.234

Local Mach numbers on wing upper surface
Rows read chordwise, and column read span wise from tip to tip

Table 5.Post-Morph: Free stream Mach number=0.9, a = 4^0

-0.038 -0.476 -0.797 -0.998 -1.085 -0.461 -0.324 -0.387 -0.373
-0.012 -0.523 -0.807 -0.987 -1.038 -0.112 -0.195 -0.261 -0.362
0.000 -0.495 -0.831 -1.002 -0.964 0.008 -0.077 -0.116 -0.096
0.021 -0.506 -0.837 -0.979 -0.773 0.003 -0.077 -0.098 -0.043
0.035 -0.509 -0.829 -0.973 -0.494 -0.077 -0.113 -0.109 -0.037
0.047 -0.510 -0.823 -0.957 -0.348 -0.090 -0.118 -0.113 -0.036
0.058 -0.509 -0.809 -0.899 -0.330 -0.068 -0.108 -0.109 -0.035
0.069 -0.504 -0.786 -0.846 -0.314 -0.057 -0.100 -0.105 -0.034
0.085 -0.491 -0.747 -0.782 -0.323 -0.056 -0.099 -0.103 -0.032
0.106 -0.465 -0.712 -0.734 -0.375 -0.023 -0.089 -0.101 -0.032
0.113 -0.456 -0.722 -0.765 -0.562 0.040 -0.063 -0.097 -0.034
0.118 -0.440 -0.716 -0.782 -0.699 0.021 -0.052 -0.089 -0.034
0.120 -0.425 -0.705 -0.804 -0.751 -0.044 -0.072 -0.089 -0.033
0.117 -0.412 -0.695 -0.785 -0.783 -0.133 -0.111 -0.102 -0.035
0.111 -0.400 -0.692 -0.769 -0.791 -0.221 -0.150 -0.120 -0.038
0.102 -0.386 -0.673 -0.778 -0.809 -0.296 -0.177 -0.137 -0.042
0.086 -0.380 -0.660 -0.774 -0.824 -0.395 -0.171 -0.146 -0.045
0.056 -0.383 -0.653 -0.784 -0.850 -0.513 -0.110 -0.123 -0.046
0.016 -0.409 -0.680 -0.832 -0.913 -0.713 0.029 -0.003 0.070

Local Pressure coefficients on wing upper surface
Rows read chordwise, and column read span wise from tip to tip

ISSN: 2454-8669

Table 6.Pre-Morph Free stream Mach number = 0.9, a = 4⁰

1.059	1.056	1.043	1.012	0.995	0.970	0.961	0.956	0.966
1.050	1.045	1.030	1.001	0.983	0.956	0.943	0.928	0.916
1.042	1.038	1.024	0.995	0.978	0.951	0.938	0.922	0.910
1.034	1.032	1.019	0.991	0.975	0.949	0.936	0.920	0.909
1.027	1.026	1.014	0.988	0.972	0.947	0.934	0.919	0.908
1.020	1.020	1.010	0.985	0.970	0.944	0.933	0.918	0.908
1.014	1.015	1.006	0.981	0.967	0.942	0.932	0.918	0.907
1.008	1.010	1.002	0.978	0.965	0.941	0.930	0.917	0.907
1.002	1.005	0.998	0.975	0.963	0.939	0.929	0.916	0.907
0.996	1.000	0.994	0.973	0.961	0.937	0.928	0.915	0.906
0.998	1.003	0.998	0.977	0.964	0.940	0.930	0.916	0.907
1.001	1.006	1.002	0.981	0.968	0.943	0.932	0.918	0.907
1.003	1.010	1.006	0.985	0.971	0.946	0.934	0.919	0.908
1.006	1.013	1.009	0.988	0.975	0.949	0.937	0.921	0.908
1.009	1.016	1.013	0.992	0.978	0.952	0.939	0.922	0.909
1.012	1.019	1.016	0.995	0.981	0.955	0.941	0.924	0.909
1.017	1.023	1.019	0.998	0.983	0.957	0.942	0.925	0.910
1.026	1.029	1.023	1.000	0.984	0.957	0.941	0.923	0.910
1.040	1.042	1.033	1.006	0.985	0.954	0.934	0.909	0.886

Local Mach numbers on wing upper surface
Rows read chord wise and column read span wise from tip to tip

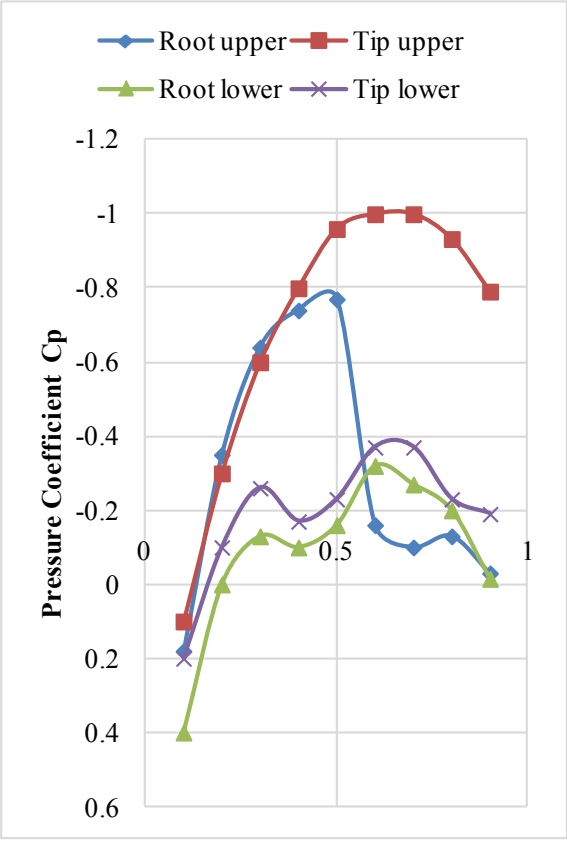

Figure 6.Chordwise pressure distributions on upper and lower surfaces, Mach no. = 0.95, a = 4⁰

Angle-of attack is increased keeping the Mach number constant at 0.95. Two angle-of-attack values are chosen namely; 4^0 and 8^0. The chord wise pressure distributions for the upper and lower surfaces on post-morph wings are plotted in Fig. 6 and 7. The plots are made for two stations, namely; root and tip. Lower surfaces have subsonic local flows. Upper surfaces have mixed flows i.e., supersonic and subsonic. The shock wave is evident by the drop of pressure. This however is seen not happening towards the wing tips, as explained earlier that there is greater suction at such regions causing flow to continue to accelerate without deceleration in spite of presence of tip vorticity that results in induced angle-of attack which reduces effective angle of attack.

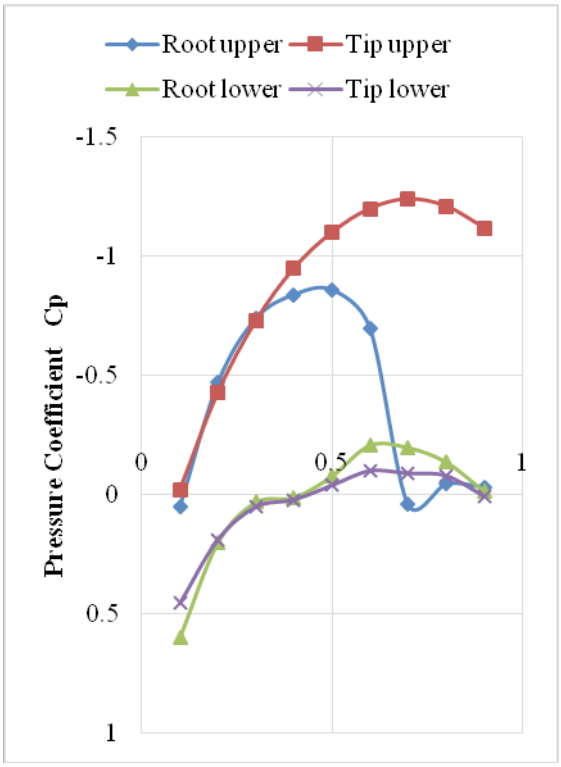

Figure 7.Chordwise pressure distribution on upper and lower surfaces, Mach no. = 0.95, a = 8^0

Wing is now designed using CATIA software, Figure 8 to refer. The model is run on ANSYS-FLUENT. The results from ANSYS are compared with FORTRAN codes. Table-5 shows comparison of reduction in drag. There is good agreement in values.

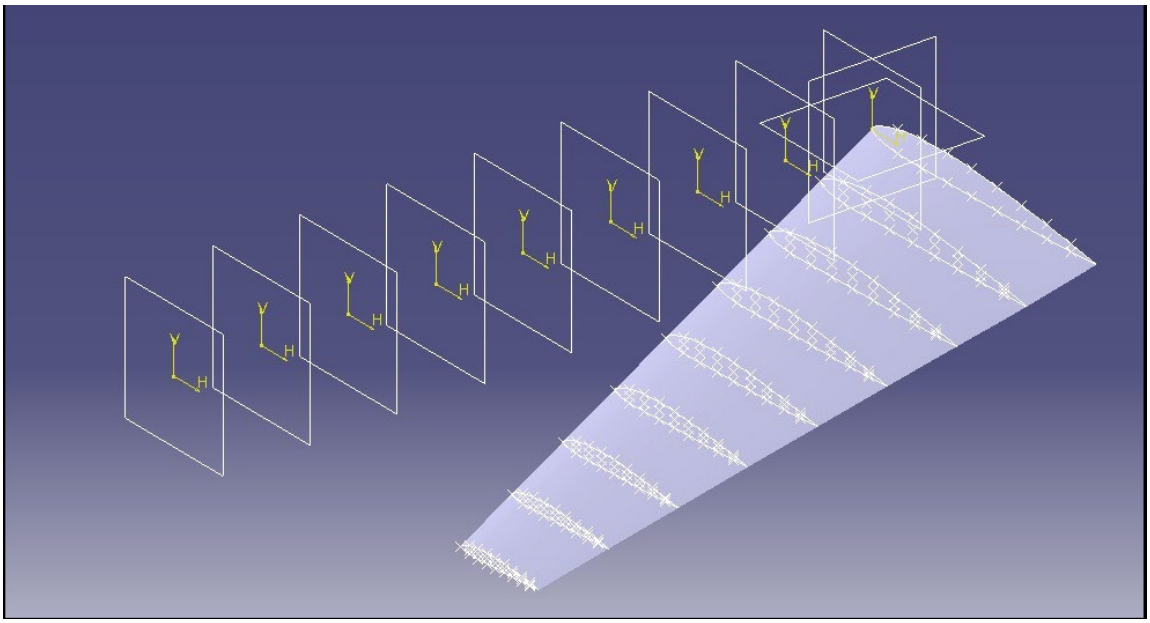

Figure 8.Final wing design through CATIA

ISSN: 2454-8669

Table 5.Result comparison between FORTRAN and ANSYS- FLUENT

Technique	C_L	Pre MorphCd_i	Post Morph Cd_i	% reduction in Cd_i
Fortran	0.279	0.0146	0.007	52.0
ANSYS-FLUENT	0.361	0.0151	0.006	59.6

Progressively varying field values of pressure coefficient near root for M=0.9 and Alpha=4^0 are shown in Fig. 9. Occurrence of shock wave appears to shift rearwards with vertical displacement. This can be seen by joining the maximum pressure coefficient values. This is what actually happens in real time flows.

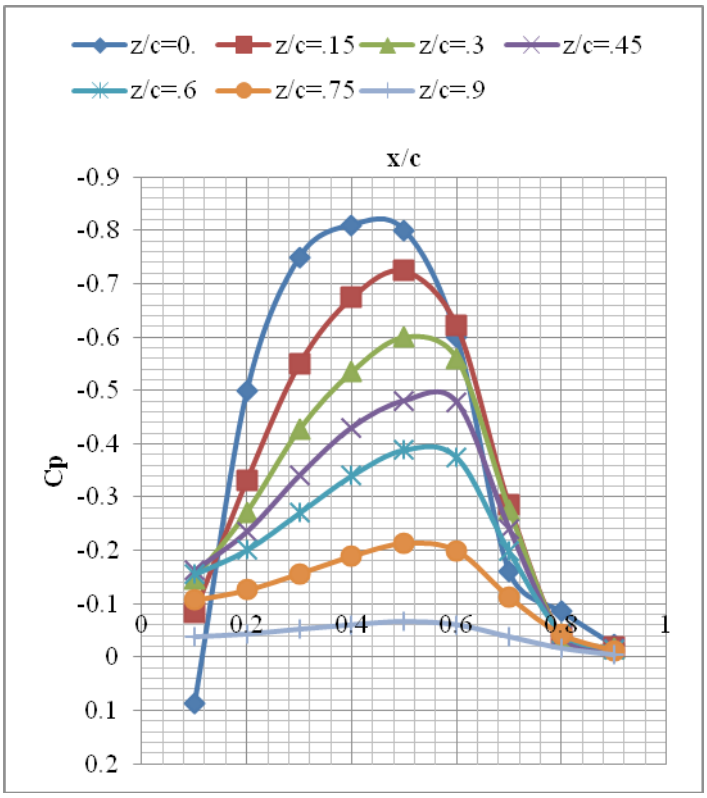

Figure 9.Progressively varying field values of pressure coefficient near root, M=0.9, Alpha=4^0

Conclusions

We are able to established process of morphing and progress transonic flow successfully. Substantial reduction in induced drag is seen possible through shaping of camber line. The flow is seen to remain supersonic towards wing tips for higher Mach number conditions.

References

1. Zhoujie L, Joaquim RRA. Strategies for solving high-fidelity aerodynamic shape optimization problems. 2014.
2. Rajesh Senthil Kumar T, Balaramraja VS. Aerodynamics of discreet location camber morphing airfoils in low Reynolds numbers flows. Indian Journal of Science and Technology 2017; 10(10).
3. Vasista S, Tung L, Wong K. Realisation of morphing wings: a multidisciplinary challenge. Journal of Aircraft 012; 49(1).
4. Fincham JHS, Friswell MI. Aerodynamic optimization of a camber morphing airfoil. Aerospace Science and Technology 2015; 43.
5. Gupta SC. GENMAP: Computer Code for Mission Adaptive Profile Generation. Journal of Aircraft 1988; 25(8).
6. Gupta SC. Aerodynamic optimisation of a camber morphing 3-D aerofoil in the presence of trailing edge flap deflection. Journal of Advance Research in Aeronautics and Space Sciences 2016; 3(4).
7. Ayers TG, Hallissy JB. Historical background and design evolution of transonic aircraft technology supercritical wing. 1981.